Anal. Chem. **2005,** *77,* 486−494

Single-Molecule Studies of Diffusion by Oligomer-Bound Dyes in Organically Modified Sol−Gel-Derived Silicate Films

Skylar A. Martin-Brown, Yi Fu, Ginagunta Saroja, Maryanne M. Collinson,* and Daniel A. Higgins*

Department of Chemistry, Kansas State University, 111 Willard Hall, Manhattan, Kansas 66506

Single-molecule fluorescence spectroscopy is used to study dye diffusion within organically modified silicate (ORMOSIL) films. ORMOSIL films are prepared from sols containing tetraethoxysilane and isobutyltrimethoxysilane in 2:1 and 1:9 molar ratios. Nile red and a new silanized form of nile red that can be covalently attached to the silicate matrix are used as fluorescent probe molecules. The number and rate of single molecules diffusing through these films increases dramatically with increasing film organic content. Autocorrelation of the fluorescence images yields a quantitative measure of the relative populations of fixed and diffusing species. Surprisingly, both "free" and silicate-bound nile red exhibit relatively facile translational motions. Single-molecule/single-point fluorescence correlation spectroscopy (FCS) is used to measure the dye diffusion coefficients in submicrometer-scale film regions. The most common diffusion coefficients for "free" and silicate-bound nile red molecules in the 1:9 films are 3.9×10^{-10} and 1.6×10^{-10} cm^2/s, respectively. The unexpectedly rapid diffusion of silicate-bound nile red is attributed to the presence of liquidlike silicate oligomers in the films. A lower bound for the molecular weight of the oligomers is estimated at 2900. Bulk solution-phase FCS experiments performed on "free" and silicate-bound nile red species extracted into chloroform solutions provide valuable support for these conclusions. Comparison of the results derived from experimental and simulated time transients indicates film heterogeneity occurs on sub-100-nm-length scales and likely results from the presence of inorganic- and organic-rich domains.

The sol−gel process provides a convenient approach to prepare technologically important silicate materials.[1−3] Relatively simple inorganic silicate matrixes can be made via the acid-catalyzed hydrolysis and condensation of tetraethoxysilane (TEOS).[1−3] More complex organically modified silicate materials (ORMOSILs) can be prepared from mixtures of organoalkoxysilanes $RSi(OR')_3$ and alkoxysilanes, where R represents different organic functional groups such as alkyl chains, aromatic rings, amines, thiols, and epoxys.[4−6] The preparation of such organic/inorganic composites provides a means to produce silicate materials with continuously tunable chemical and physical properties by simply changing the precursors employed, their molar ratios, or both. ORMOSIL materials with tailored hydrophobicity, flexibility, reactivity, porosity, and stability have previously been described,[4−6] as have their applications in the areas of ion exchange materials,[7] chemical sensors,[8−10] catalysts,[11−14] and stationary phases for chromatographic separations.[15,16]

Of utmost importance to these applications is the rate at which reagents and encapsulated guests move through the material of choice. Diffusion in sol−gel-derived materials, however, can be very complicated.[17−21] Dopant−matrix interactions, matrix porosity, and pore interconnectivity all influence diffusion in sol−gel-derived matrixes.[17−20] One powerful method for studying diffusion of dyes in thin films or on their surfaces is fluorescence correlation spectroscopy (FCS).[21−26] FCS methods have been applied previously in studies of silicate materials. For example, Dai and coworkers have studied the diffusion of rhodamine 6G in mesoporous silicate glasses.[23] Their results showed that diffusion through these materials occurred on two distinct time scales. The fast component was attributed to the motions of "free" molecules, while

* Corresponding authors. E-mail: mmc@ksu.edu; higgins@ksu.edu.

(1) Brinker, J.; Scherer, G. *Sol−Gel Science*; Academic Press: New York, 1989.
(2) Avnir, D. *Acc. Chem. Res.* **1995**, *28*, 328.
(3) Collinson, M. M. Structure, Chemistry, and Applications of Sol−Gel Derived Materials. In *Chalcogenide Glasses and Sol−Gel Materials*; Nalwa, H. S., Ed.; Academic Press: New York, 2001; Vol. 5; p 163.
(4) Wen, J.; Wilkes, G. L. *Chem. Mater.* **1996**, *8*, 1667.
(5) Collinson, M. M. *Trends Anal. Chem.* **2002**, *21*, 30.
(6) Schmidt, H. *J. Sol-Gel Sci. Technol.* **1994**, *1*, 217.
(7) Wei, H.; Collinson, M. M. *Anal. Chim. Acta* **1999**, *397*, 113.
(8) Wolfbeis, O. S.; Reisfeld, R.; Oehme, I. Sol Gels and Chemical Sensors. In *Structure and Bonding*; Springer-Verlag: Berlin, 1996; Vol. 85; p 51.
(9) Lin, J.; Brown, C. W. *Trends Anal. Chem.* **1997**, *16*, 200.
(10) Dave, B. C.; Dunn, B.; Valentine, J. S.; Zink, J. I. *Anal. Chem.* **1994**, *66*, 1120A.
(11) Blum, J.; Avnir, D.; Schumann, H. *Chemtech* **1999**, 32.
(12) Gelman, F.; Avnir, D.; Schumann, H.; Blum, J. *J. Mol. Catal. A* **1999**, *146*, 123.
(13) Abu-Reziq, R.; Avnir, D.; Blum, J. *J. Mol. Catal. A* **2002**, *187*, 277.
(14) Sandee, A. J.; Reek, J. N. H.; Kamer, P. C. J.; van Leeuwen, P. W. N. M. *J. Am. Chem. Soc.* **2001**, *123*, 8468.
(15) Rodriguez, S. A.; Colon, L. A. *Chem. Mater.* **1999**, *11*, 754.
(16) Wang, D.; Chong, S. L.; Malik, A. *Anal. Chem.* **1997**, *69*, 4566.
(17) Howells, A. R.; Zambrano, P. J.; Collinson, M. M. *Anal. Chem.* **2000**, *72*, 5265.
(18) Watson, J.; Zerda, T. W. *Appl. Spectrosc.* **1991**, *45*, 1360.
(19) Koone, N.; Shao, Y.; Zerda, T. W. *J. Phys. Chem.* **1995**, *99*, 16976.
(20) McCain, K. S.; Hanley, D. C.; Harris, J. M. *Anal. Chem.* **2003**, *75*, 4351.
(21) McCain, K. S.; Schluesche, P.; Harris, J. M. *Anal. Chem.* **2004**, *76*, 939.
(22) Elson, E. L.; Magde, D. *Biopolymers* **1974**, *13*, 1.
(23) Mahurin, S. M.; Dai, S.; Barnes, M. D. *J. Phys. Chem. B* **2003**, *107*, 13336.
(24) Wirth, M. J.; Swinton, D. J. *Anal. Chem.* **1998**, *70*, 5264.
(25) Wirth, M. J.; Swinton, D. J. *J. Phys. Chem. B* **2001**, *105*, 1472.
(26) Wirth, M. J.; Ludes, M. D.; Swinton, D. J. *Appl. Spectrosc.* **2001**, *55*, 663.

10.1021/ac0491511 CCC: $30.25
Published on Web 12/07/2004

slow diffusion was assigned to molecules adsorbing/desorbing from the surface or becoming entrapped in pores. Diffusion in silicate films prepared from silica particles has been studied by McCain and Harris, using total internal reflection FCS[21] and single-molecule tracking.[20] Their results point to micrometer-scale variations in the diffusion coefficients observed for dye molecules and dye-labeled dendrimers. Importantly, the level of heterogeneity observed varied inversely with the size of the diffusing species. Swinton and Wirth have also used FCS methods to examine lateral diffusion and rare strong adsorption in C_{18} phases fused onto silica surfaces in contact with aqueous solutions.[24,25] Their results point to the presence of reactive sites on the silica surfaces, to which the molecules can periodically bind.

As demonstrated by some of the aforementioned examples, it is now possible to study diffusion (e.g., mass transport) at the single-molecule level.[27−29] Single-molecule methods offer several unique advantages over more common bulk physical methods for studying diffusion. Most importantly, single-molecule methods eliminate the averaging associated with bulk methods. As a result, spatial variations in the properties of heterogeneous materials can be directly probed. Since sol−gel-derived hybrid organic/inorganic composites are known to be heterogeneous,[30] single-molecule methods may be able to help unravel some of the complexities associated with dopant diffusion.

In this paper, FCS at the single-molecule/single-point level is used to examine diffusion in organic/inorganic hybrid silicate films prepared by the sol−gel process. Such films likely incorporate phase-separated domains of inorganic- and organic-rich silicate materials.[31−36] In earlier studies from our research program, it was shown that dye molecules entrapped in hybrid silicates of high organic content exhibited unexpectedly facile translational diffusion.[31,32] At lower organic content, the dye molecules appeared to be entrapped at fixed sites within the films. The percentage of molecules that appeared to diffuse was observed to increase with increasing film organic content. However, the diffusion of these molecules was not quantitatively explored in these previous studies, which focused primarily on film polarity properties and the possibility of phase separation of the inorganic and organic film components.

The main objectives of the present studies include a much more quantitative understanding of the mechanism and rates of probe diffusion through these materials, as well as more complete information on the level of film heterogeneity as it relates to probe diffusion. To this end, two different dye molecules are employed as single-molecule probes of the diffusion process. Nile red (NR) is employed as a probe of "free" diffusion through the films. The results are compared to those obtained from a silanized form of nile red (NR-Si) that covalently binds to the silicate matrix when cohydrolyzed and cocondensed with the precursor silanes. Figure 1 shows the chemical structures of these two dyes. Diffusion is studied in two classes of film: one derived from sols of low (33 mol %) organic content and the other from sols of high (90 mol %) organic content. These two films are representative of the extremes observed in our previous studies;[31,32] no apparent diffusion is observed in the first, while facile diffusion occurs in the second. The results of these studies indicate that liquidlike silicate oligomers are present in the organic/inorganic hybrids and that these oligomers allow for diffusion of even the silicate-bound dye. The results of bulk diffusion studies in which the "free" and silicate-bound forms of NR are extracted from the films into chloroform solution provide strong support for these conclusions.

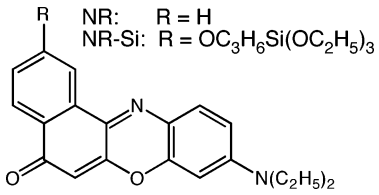

Figure 1. Chemical structures of nile red (NR) and the silanized form of nile red (NR-Si).

EXPERIMENTAL SECTION

Sample Preparation. *Nile Red Samples.* ORMOSIL films were prepared from sols containing TEOS (Aldrich 99+%) and isobutyltrimethoxysilane (BTMOS, Fluka 95%). The precursor sols were composed of either 67 mol % TEOS and 33 mol % BTMOS (2:1 molar ratio) or 10 mol % TEOS and 90 mol % BTMOS (1:9 molar ratio). In both cases, the sols were prepared in 1:4:5:0.006 (total silane/ethanol/water/HCl) mole ratios. Each sol was stirred for ~30 min after addition of all ingredients. The sols were then allowed to stand for ~48 h at 33% humidity. For the single-molecule experiments, a methanolic solution of NR (Aldrich) was then added to each to yield a total dye concentration of 0.5 nM. Immediately after addition of the dye, 100 μL of the sol was spin cast under nitrogen onto a cleaned glass microscope coverslip (Fisher Premium). Films of 350−550-nm thickness were obtained.[31] The films were dried in a desiccator overnight prior to use. All single-molecule experiments were conducted under dry air (20% relative humidity) at room temperature. Experiments were performed on each sample for ~6−8 h.

Silanized Nile Red Samples. Sols were prepared as described above. However, for these samples, a methanolic solution of NR-Si was added immediately after the initial stirring of the sol. NR-Si was synthesized as described below. The dye-doped sol was allowed to stand for 48 h, spin cast, and dried in a manner identical to the NR-doped films.

Samples for Bulk Diffusion Studies. Thin films were generally prepared as described above, from 90 mol % BTMOS sols. However, more dye (NR or NR-Si) was added to each sol to yield a final dye concentration of 10 nM in each case. Once the films had been cast and dried, the entrapped dye molecules were extracted into chloroform solution. This was accomplished by transferring each sample to a small vial, to which 100 μL of chloroform was subsequently added. The vials were then capped and shaken vigorously for several minutes. This procedure was

(27) Dickson, R. M.; Norris, D. J.; Tzeng, Y.-L.; Moerner, W. E. *Science* **1996**, *274*, 966.
(28) Schmidt, T.; Schütz, G. J.; Baumgartner, W.; Gruber, H. J.; Schindler, H. *Proc. Natl. Acad. Sci. U.S.A.* **1996**, *93*, 2926.
(29) Schütz, G. J.; Schindler, H.; Schmidt, T. *Biophys. J.* **1997**, *73*, 1073.
(30) Dunn, B.; Zink, J. I. *Chem. Mater.* **1997**, *9*, 2280.
(31) Bardo, A. M.; Collinson, M. M.; Higgins, D. A. *Chem. Mater.* **2001**, *13*, 2713.
(32) Higgins, D. A.; Collinson, M. M.; Saroja, G.; Bardo, A. M. *Chem. Mater.* **2002**, *14*, 3734.
(33) Brennan, J. D.; Hartman, J. S.; Ilnicki, E. I.; Rakic, M. *Chem. Mater.* **1999**, *11*, 1853.
(34) Keeling-Tucker, T.; Brennan, J. D. *Chem. Mater.* **2001**, *13*, 3331.
(35) Frenkel-Mullerad, H.; Avnir, D. *Chem. Mater.* **2000**, *12*, 3754.
(36) Rottman, C.; Grader, G.; Avnir, D. *Chem. Mater.* **2001**, *13*, 3631.

Scheme 1. Synthesis of 9-Diethylamino-2-(triethoxysilyl-3-propyloxy)-5*H*-benzo[α]phenoxazin-5-one (NR-Si)

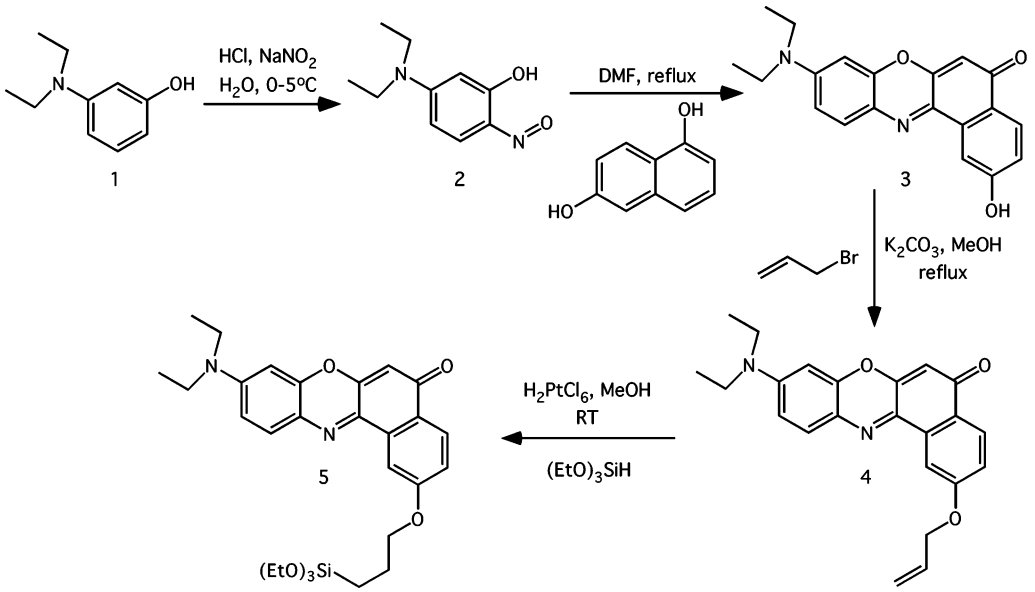

repeated three times for each vial, using three films of each type. A small quantity of the chloroform solution containing the extracted dye was then deposited onto a microscope cover glass. A second cover glass was placed on top to spread the solution and to prevent its evaporation. The sample was then immediately transferred to the microscope for characterization.

Instrumentation. *Single-Molecule Imaging and Diffusion Studies.* All single-molecule studies were conducted on a sample scanning confocal microscope described previously.[31,32] Briefly, the system was built around an inverted microscope (Nikon TE-200). Light from a green helium−neon laser (543 nm) was used as the excitation source. The excitation beam first passed through a 543-nm band-pass filter (CVI, 10-nm pass-band), polarization control optics, and a telescope, before being directed into the epi-illumination port of the microscope. A dichroic beam splitter (Chroma 565DCLP) was used to reflect the excitation light into the back aperture of the oil immersion objective (Nikon Plan Fluor, 1.3 numerical aperture, 100×). This system produces a nearly diffraction limited Gaussian spot of width $s \approx 200$ nm in the sample. The incident laser power was always maintained in the 200−400-nW range. The sample was mounted above the objective on a piezoelectric scanning stage (Queensgate) employing closed-loop feedback in *X* and *Y*. The software used to control the stage and collect images and time transients was written in-house.

The fluorescence emitted by single molecules was collected by the same oil immersion objective. Emission to the red of 565 nm passed through the dichroic beam splitter and was directed into the detection path. To further isolate single-molecule emission and reduce background, a 100-nm-wide band-pass filter centered at 650 nm was also employed. A single photon counting avalanche photodiode was used as the detector. Images were recorded by raster scanning the sample above the focused spot of the incident laser. The fast-scan direction is oriented horizontally on all images reported herein, while the slow-scan direction corresponds to vertical on the images. Raster scanning was performed in a bidirectional fashion so that the individual line scans were recorded in alternating (i.e., left-to-right and right-to-left) directions. The fluorescence signal was integrated for 40 ms/pixel in the 100 × 100 pixel images. Single-point time transients were obtained by positioning selected sample regions in the laser focus and recording the spectrally integrated fluorescence in time. These latter experiments employed a dwell time of 10 ms. The total length of the time transients recorded was 670 s in the case of NR and 1340 s for NR-Si. The results of computer simulations described below indicated these transient lengths were sufficient for accurate measurement of the relevant diffusion coefficients.

Bulk Solution-Phase Fluorescence Correlation Spectroscopy. Fluorescence time transients from bulk solutions of the dyes were recorded using the confocal microscope. For these measurements, however, a fast multichannel scaler (Perkin-Elmer) was employed to record the transients with much better (50 μs) time resolution. In addition, the incident laser power into the microscope was increased to ∼200−400 μW to obtain sufficient signal from the dye molecules as they diffused through the focal volume of the microscope. Finally, to ensure the data obtained were from diffusion in bulk solution (avoiding surface effects), the microscope focus was positioned between the two glass/solution interfaces, which were separated from each other by distances ranging from 10 to 40 μm.

Synthesis of Silanized Nile Red. A four-step procedure was required to obtain NR-Si. The entire synthesis is outlined in Scheme 1.[37]

*Synthesis of 5-(Diethylamino)-2-nitrosophenol (**2**).* *m*-Diethylaminophenol (6 g, 0.0363 mol, Aldrich, **1**) was dissolved in a mixture of 13 mL of HCl and 8 mL of water. The solution was cooled to 0 °C while stirring. To this cold solution, a solution of $NaNO_2$ (2.5 g, 0.036 mol) in 18 mL of water was added dropwise over a period of 30 min, while maintaining a temperature of 0−5 °C. A vigorous exothermic reaction occurred. Once the addition was complete, the reaction mixture was stirred at 0−5 °C for an additional 4 h. The crude HCl salt was collected by filtration and

(37) Briggs, M. S. J.; Bruce, I.; Miller, J. N.; Moody, C. J.; Simmonds, A. C.; Swann, E. *J. Chem. Soc., Perkin Trans. 1* **1997**, 1051.

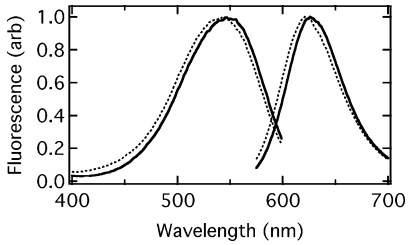

Figure 2. Fluorescence excitation and emission spectra of NR (—) and NR-Si (- - -). All spectra were taken in spectrophotometric grade ethanol with a dye concentration of 1 μM.

dried under reduced pressure for 8 h at 50 °C. The product was dissolved in 100−200 mL of boiling ethanol and then cooled to 40°C. Diethyl ether was slowly added until crystallization began. The mixture was cooled to 5 °C and kept refrigerated for 1 day. Finally, the product was collected by filtration and dried to yield 4.9 g (70%) of the title compound.

*Synthesis of 9-Diethylamino-2-hydroxy-5H-benzo[a]phenoxazin-5-one (**3**).* 1,6-Dihydroxynaphthalene (0.725 g, 4.53 mmol) and **2** (1 g, 4.53 mmol) were heated under reflux in DMF (100 mL) for 4 h. The solvent was removed by rotary evaporation. The crude product was purified by column chromatography using 5:2 ethyl acetate/2-propanol to yield 1.5 g (60%) of the title compound as a green solid: ^{1}H NMR δ_H (400 MHz, DMSO-d_6) 10.46 (1H, br, OH), 7.95 (1H, d, 4-H), 7.88 (1H, d, 1-H), 7.58 (1H, d, 11-H), 7.10 (1H, dd, 3-H), 6.80 (1H, dd, 10-H), 6.64 (1H, d, 8-H), 6.15 (1H, s, 6-H), 3.49 (4H, q, N(CH_2CH$_3$)$_2$) and 1.20 (6H, t, N(CH$_2$CH_3)$_2$).

*Synthesis of 9-Diethylamino-2-allyloxy-5H-benzo[a]phenoxazin-5-one (**4**).* Allyl bromide (0.5 mL, 5 mmol) and **3** (500 mg, 1.5 mmol) were dissolved in anhydrous methanol to which excess K_2CO_3 was added. The reaction mixture was refluxed for 48 h. After evaporation of the solvent, the crude product was purified by column chromatography using 3:1 hexane/ethyl acetate to give the title compound as a purple solid: ^{1}H NMR δ_H (400 MHz, $CDCl_3$) 8.21 (1H, d, 4-H), 8.06 (1H, d, 1-H), 7.59 (1H, d, 11-H), 7.17 (1H, dd, 3-H), 6.65 (1H, dd, 10-H), 6.45 (1H, d, 8-H), 6.29 (1H, s, 6-H), 6.1 (1H, m, OCH$_2$CH=CH$_2$), 5.49 (1H, d, OCH$_2$CH=CH_2), 5.33 (1H, d, OCH$_2$CH=CH_2), 4.73 (2H, d, OCH_2CH=CH$_2$), 3.45 (4H, q, N(CH_2CH$_3$)$_2$), and 1.25 (6H, t, N(CH$_2$CH_3)$_2$).

*Synthesis of 9-Diethylamino-2-(triethoxysilyl-3-propyloxy)-5H-benzo[a]phenoxazin-5-one (**5**, NR-Si).*[38] Compound **4** (80 mg, 0.21 mmol) was dissolved in 20 mL of anhydrous methanol in a round-bottom flask. The flask was fitted with a condenser and drying tube and heated to reflux. To the warm solution, 15 mg of H_2PtCl_6 dissolved in a few drops of 2-propanol was added, followed by HSi(OCH$_2$CH$_3$)$_3$ (0.7 g, 4.3 mmol) 10 min later. The solution quickly changed from purple to brown upon silane addition. At this point, heating was terminated and the flask was wrapped in aluminum foil. The solution was subsequently stirred under dry nitrogen for 36 h. The solvent was removed by rotary evaporation to give the title compound. The product was stored in a drybox or desiccator: ^{1}H NMR δ_H (400 MHz, $CDCl_3$) 8.23 (1H, d, 4-H), 8.07 (1H, d, 1-H), 7.63 (1H, d, 11-H), 7.18 (1H, dd, 3-H), 6.68 (1H, dd, 10-H), 6.48 (1H, d, 8-H), 6.32 (1H, s, 6-H), 4.16 (2H, t, OCH_2CH$_2$CH$_2$Si), 3.74 (6H, q, Si(OCH_2CH$_3$)$_3$), 3.49 (4H, q, N(CH_2CH$_3$)$_2$), 1.90 (2H, m, OCH$_2$CH_2CH$_2$Si), 1.33 (9H, t, Si(OCH$_2$CH_3)$_3$), 1.25 (6H, t, N(CH$_2$CH_3)$_2$), 1.11 (2H, t, OCH$_2$CH$_2$CH_2Si).

(38) Leventis, N.; Chen, M. *Chem. Mater.* **1997**, *9*, 2621.

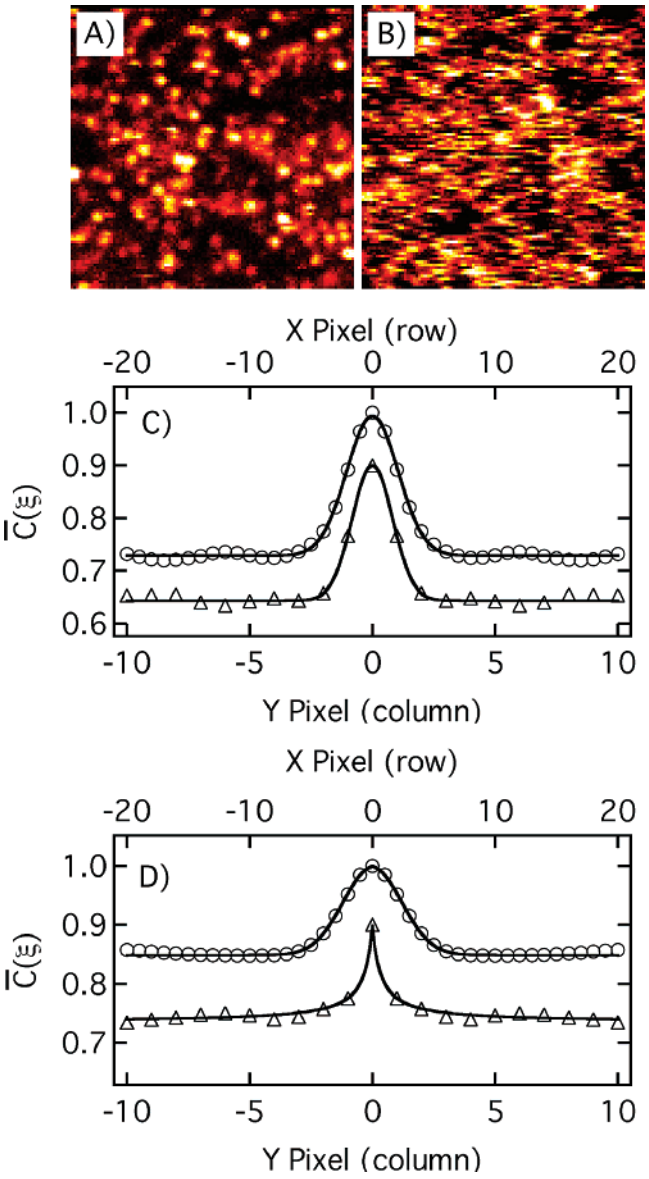

Figure 3. Fluorescence images of (A) a 33% BTMOS film doped with NR and (B) a 90% BTMOS film doped with NR-Si. Both images are of 10 × 10 μm regions. (C, D) Autocorrelations along the horizontal (circles) and vertical (triangles) directions for the images shown in (A) and (B), respectively. Fits to the autocorrelation functions in each case are depicted by the solid lines. The vertical autocorrelation data have been offset in the *y*-direction. Average values for the amplitudes of the Gaussian and diffusional decay components (A_g and A_d, respectively) can be found in the main text.

RESULTS AND DISCUSSION

Fluorescence Spectra for NR and NR-Si. Figure 2 depicts the fluorescence spectra obtained from NR and NR-Si in bulk ethanol solution. Aside from a subtle blue shift for NR-Si, the two dyes exhibit nearly identical fluorescence excitation and emission spectra. Each is most efficiently excited near 550 nm, and each emits most strongly near 625 nm. These results indicate that the two dyes will exhibit similar fluorescence characteristics when

probed in silicate films. Any differences observed between NR and NR-Si single molecules may therefore be attributed to differences in the interactions of the dye with the silicate matrix. The NR-Si dye was prepared specifically for covalent attachment to the matrix. Numerous studies have shown that similar organoalkoxysilanes can be chemically attached to the matrix by cohydrolysis and cocondensation with another silicon alkoxide.[14,38–43]

Imaging and Spatial Autocorrelations. Figure 3A shows a representative fluorescence image of a 33% BTMOS film doped with NR, while Figure 3B depicts such an image for a NR-Si-doped 90% BTMOS film. NR-Si-doped 33% BTMOS films and NR-doped 90% BTMOS films yield images that are nearly indistinguishable by eye from those shown in Figure 3A and B, respectively. Examples are given in the Supporting Information (Figure S-1). These images are consistent with those obtained in previous studies of a series of NR-doped hybrid silicate films prepared from sols having a range of TEOS/BTMOS ratios.[31,32] Regardless of the specific form of NR employed, images obtained from films of low BTMOS content are composed of bright round fluorescent spots, consistent with the excitation and emission of single molecules entrapped at fixed positions within the films. In contrast, images obtained from films of high organic content (i.e., >66% BTMOS)[31] exhibit dramatic line-by-line variations in single-molecule emission, whether they are doped with NR or NR-Si. Previous studies have shown that translational diffusion is a major contributor to the "streaky" appearance of these images.[31,32] It is most surprising that the NR-Si molecules exhibit what is apparently facile translational diffusion (see Figure 3B), since they are expected to be bound to the silicate matrix.

The "streaks" in such images result from a combination of spatial and temporal contrast (referred to below as "spatiotemporal" contrast) associated with the mobile molecules. In these experiments, the images are recorded by sample-scanning methods. The horizontal direction on each image represents the "fast-scan" direction. Images are constructed by recording a series of individual line scans in the fast-scan direction for a series of positions along the vertical direction. The vertical direction on an image represents the "slow-scan" direction. Individual image pixels along the horizontal direction are recorded at 40-ms intervals, while the image pixels along the vertical direction (in alternating horizontal lines) are separated by 8 s (the latter complexity arises from the bidirectional nature of the fast scan axis). Hence, the data in the horizontal and vertical image directions incorporate temporal information on two distinct time scales. Molecules may appear in a fixed position for a single horizontal line scan and subsequently move to a new position prior to the recording of the next line scan. Images incorporating narrow horizontal fluorescent streaks result, reflecting temporal variations in the positions of mobile molecules. The horizontal widths of these streaks are often governed by diffraction-limited excitation of the molecules, while their vertical widths reflect the rates of temporal variation in their positions.

Autocorrelation of these fluorescence images[44] can then be used to determine the relative contributions of fixed and mobile molecules to the signal fluctuations ("spatiotemporal" contrast) observed. Representative autocorrelations are shown in Figure 3, along with the images from which they were derived. These image autocorrelations were calculated as follows:[44]

$$C(\xi) = \langle i(x)i(x+\xi)\rangle/\langle i(x)^2\rangle \qquad (1)$$

where $i(x)$ represents an intensity trace along the horizontal (x) direction in an image. A similar expression defines the autocorrelation in the vertical (y) direction. Again, the x and y coordinates in these image autocorrelations contain both spatial and temporal information. The brackets (< >) indicate the average over all points in each trace is taken. The autocorrelation functions plotted in Figure 3 represent average autocorrelation functions, $\bar{C}(\xi)$, obtained by averaging all autocorrelation functions in the horizontal and vertical directions for each image. As noted above, the images were recorded by raster scanning the sample in a bidirectional fashion. Therefore, to maintain a constant temporal separation (8 s) between the data points in the vertical image direction, alternate pixels were employed to produce two separate autocorrelations along the vertical direction for each image. This process results in a 2-fold reduction in the data density. All such autocorrelations were then averaged together for use in Figure 3.

To obtain a measure of the relative contributions of fixed and mobile molecules to the signal fluctuations in the images, the autocorrelations calculated above were fit with an approximate decay function. For this model, variations in the signal were assumed to arise from fixed molecules, whose intensities fall off spatially with a Gaussian (i.e., diffraction-limited) profile, and diffusing molecules, whose intensities fluctuate more rapidly because of their time-dependent motions. Hence, the fitting expression combines both Gaussian and diffusional decays as follows:[23,25,45]

$$\bar{C}(\xi) = \frac{A_d}{(1 + D'|\xi|)} + A_g \exp\left(-\left(\frac{\xi}{2s}\right)^2\right) + B \qquad (2)$$

In eq 2, A_d and A_g are the amplitudes of the decays associated with diffusing and fixed species, respectively. D' is related to the diffusion coefficient of the molecule, the scan rate, and the beam variance but is treated here simply as a fitting parameter (i.e., it was not used to determine the diffusion coefficient), s^2 is the variance of the focused laser beam used to excite the molecules, and B is a constant. The value used for s (1.9×10^{-5} cm) was determined by fitting the 33% BTMOS image autocorrelations to eq 2. In fitting the 90% BTMOS data, its value was held fixed to within 25% to allow for variations in the microscope focus. The relative contributions of fixed and diffusing molecules to the spatial signal fluctuations were then obtained from the relative amplitudes

(39) Pandey, S.; Baker, G. A.; Kane, M. A.; Bonzagni, N. J.; Bright, F. V. *Chem. Mater.* **2000**, *12*, 3547.
(40) Chambers, R. C.; Haruvy, Y.; Fox, M. A. *Chem. Mater.* **1994**, *6*, 1351.
(41) Suratwala, T.; Gardlund, Z.; Davidson, K.; Uhlmann, D. R.; Watson, J.; Peyghambarian, N. *Chem. Mater.* **1998**, *10*, 190.
(42) Suratwala, T.; Gardlund, Z.; Davidson, K.; Uhlmann, D. R.; Watson, J.; Bonilla, S.; Peyghambarian, N. *Chem. Mater.* **1998**, *10*, 199.
(43) Rottman, C.; Turniansky, A.; Avnir, D. *J. Sol-Gel Sci. Technol.* **1998**, *13*, 17.
(44) Petersen, N. O.; Hoddelius, P. L.; Wiseman, P. W.; Seger, O.; Magnusson, K.-E. *Biophys. J.* **1993**, *65*, 1135.
(45) Srivastava, M.; Petersen, N. O. *Biophys. Chem.* **1998**, *75*, 201.

of the two decay components as $A_g/(A_d + A_g)$ and $A_d/(A_d + A_g)$, respectively.

To properly fit the image autocorrelations, the contributions of uncorrelated shot noise to the first point, $\bar{C}(\xi = 0)$, in each was subtracted. Shot noise was removed by simply subtracting the average signal in each image from $\bar{C}(\xi = 0)$ and renormalizing the corrected autocorrelation. This process improves the autocorrelation fits dramatically, but the contributions of uncorrelated noise from other sources are still present and limit the accuracy to some degree. While such corrections are inexact, they are necessitated by the limited data density in the image autocorrelation functions.

For 33% BTMOS films doped with either NR or NR-Si, the autocorrelation functions could be fit well with $A_g = 1$ and $A_d = 0$ in every instance, indicating that the dyes remain in "fixed" locations on the time scale of the experiment. For data obtained from 90% BTMOS films, the relative contributions of fixed and mobile molecules depend on the autocorrelation direction (see Figure 3D), as well as the specific dye molecule used as the dopant. For NR in the horizontal (fast scan) direction, average values of $A_g = 0.35 \pm 0.15$ and $A_d = 0.65 \pm 0.14$ were obtained from several images. The same images yielded averages of $A_g = 0.16 \pm 0.05$ and $A_d = 0.84 \pm 0.05$ for the vertical (slow scan) direction, for those images having a nonzero A_g value. Approximately 43% of the images yielded $A_g \approx 0$ for autocorrelations in the vertical direction. For NR-Si in the horizontal direction, average values of $A_g = 0.71 \pm 0.28$ and $A_d = 0.29 \pm 0.28$ were obtained from several images, while average values of $A_g = 0.17 \pm 0.02$ and $A_d = 0.83 \pm 0.02$ were obtained in the vertical direction for those images yielding nonzero A_g values. The values obtained for A_g (and A_d) in the horizontal direction differ for NR and NR-Si at greater than the 90% confidence level. These results indicate that a significantly smaller fraction of the NR-Si molecules is "mobile" on the time scale of the horizontal line scans in 90% BTMOS samples, as expected for silicate-bound molecules.

Fluorescence Time Transients and Temporal Autocorrelations. Information on the rate of single-molecule diffusion was obtained by recording single-point fluorescence time transients. In these studies, selected points in each sample were positioned above the focused excitation spot and the integrated (total) sample fluorescence recorded as a function of time, with 10-ms resolution. These time transients were then autocorrelated and the autocorrelation functions fit to appropriate expressions, as defined below. Figure 4 shows representative results of these experiments for NR in a 33% BTMOS film (Figure 4A,B) and for NR-Si in a 90% BTMOS film (Figure 4C,D).

The signal in Figure 4A arises from a single molecule (a single round fluorescent spot) entrapped in the film at a fixed location. The shutter blocking the excitation beam was opened early in the transient, leading to the initial abrupt increase in fluorescence. Emission from this molecule remained relatively stable for a period of ~70 s. At that time, an irreversible transition to a dark state was observed, likely due to photodestruction of the chromophore. This particular molecule survived longer than most molecules in these materials, which typically last no more than several seconds. However, the "constant" emission observed prior to photobleaching is representative of typical single molecules in films of low BTMOS content.[31]

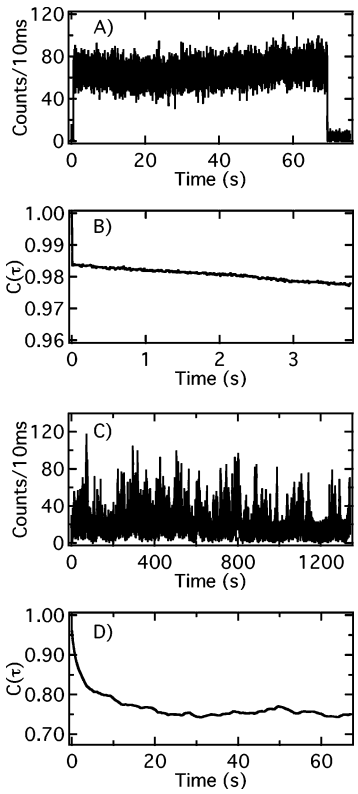

Figure 4. Representative single-point fluorescence time transients and their autocorrelations. (A, B) For NR in a 33% BTMOS film. (C, D) for NR-Si in a 90% BTMOS film.

NR and NR-Si in 90% BTMOS films yielded time transients dramatically different from the single molecules entrapped in 33% BTMOS films (see Figure 4C,D). In 90% BTMOS films, the fluorescence time transients exhibited large-amplitude, rapid signal fluctuations over much longer periods of time (the longest time transients recorded for NR-Si were 22.3 min in length). No clear evidence of single-molecule photobleaching was observed for either NR or NR-Si, even for these extremely long transients. Such an observation represents strong evidence for relatively facile diffusion of different single molecules in to and out of the excitation region of the microscope, even in the case of the silicate-bound NR-Si.

The fluorescence time transients recorded for NR and NR-Si single molecules in the 33% BTMOS films and for single locations in the 90% BTMOS films were used to calculate autocorrelation functions as follows:

$$C(\tau) = \langle i(t)i(t+\tau)\rangle/\langle i(t)^2\rangle \qquad (3)$$

where $i(t)$ represents the fluorescence time transient. Autocorrelations obtained from fixed molecules in the 33% BTMOS films were usually fit to exponential decays in order to obtain a measure of the characteristic time scales for their signal fluctuations.[31] Of primary interest here, however, are the diffusion coefficients associated with single molecules diffusing in to and out of the excitation region in the 90% BTMOS films. In this case, the autocorrelations were fit with the following equation:[23−26]

$$C(\tau) = \frac{A_1}{(1 + D_1\tau/s^2)} + \frac{A_2}{(1 + D_2\tau/s^2)} + B \qquad (4)$$

Here, D_1 and D_2 are diffusion coefficients associated with two separate diffusional decays, A_1 and A_2 are the amplitudes of these two decays, and s^2 is the variance of the excitation region in the microscope ($s^2 = 3.7 \times 10^{-10}$ cm^2). In fitting these temporal autocorrelations, the first point in each, $C(\tau = 0)$, was simply excluded from the fit, rather than attempting a correction as in the case of the image autocorrelations. Also, only the first 5% of each autocorrelation was fit, since insufficient information on longer time-scale fluctuations exists in these data.[46] A majority of the autocorrelations (67% in the case of NR and 50% in the case of NR-Si) analyzed herein required two separate diffusional components to properly fit the observed decays, as shown in eq 4.[23] A minority of the autocorrelations could, however, be fit with a single component (i.e., $A_2 = 0$ in eq 4). Previously, a combination of diffusional and exponential decays have been employed to fit transients that exhibited both diffusion and strong adsorption of single molecules on similar surfaces.[24−26] However, the transients recorded for 90% BTMOS films do not show evidence of long-term adsorption, and hence, the present data have been interpreted to reflect diffusional processes alone. In reality, the signal-to-noise ratio in most autocorrelations is too small to distinguish between these two models based solely on the quality of the fit.[23]

Autocorrelations from 123 sites in NR-doped 90% BTMOS samples and 112 sites in NR-Si-doped samples were fit to obtain measurements of their respective diffusion coefficients. Figure 5 depicts histograms showing the full inhomogeneous distributions for both the fast- and slow-diffusion components (D_1 and D_2, from eq 4) observed in the data. The histograms given in Figure 5A,B (fast diffusion component) were fit to Gaussian functions to determine the peak of each distribution and, hence, the most common diffusion coefficient observed in each sample. NR-doped 90% BTMOS samples yielded $D_{peak} = 3.9 \times 10^{-10}$ cm^2/s and the NR-Si-doped samples $D_{peak} = 1.6 \times 10^{-10}$ cm^2/s. The average D values obtained by numerically averaging all values obtained for each sample were 1.2×10^{-9} and 2.9×10^{-10} cm^2/s, respectively. Hence, "free" NR diffusion through the films is only ~3−4 times faster than silicate-bound NR-Si. Similarly subtle differences in the rotational mobilities of silicate-bound and unbound pyrene molecules have been reported previously by Fox and co-workers.[40] The small difference observed here suggests that the 90% BTMOS films are best described as a "fluid" matrix, possibly incorporating liquidlike organosilicate oligomers. These oligomers likely result from incomplete condensation of the hydrolyzed organoalkoxysilanes and would facilitate the translational motions of "free" NR. In the case of silicate-bound NR-Si, it is hypothesized that the diffusing species is actually a silicate-oligomer-bound NR-Si.

Bulk solution-phase FCS experiments were undertaken to test the latter hypothesis. In these studies, time transients for bulk chloroform solutions of both dyes were recorded and autocorrelated in order to obtain a measure of their solution-phase diffusion coefficients. Figure S-2 in the Supporting Information presents example results. Two different types of solution-phase samples were characterized. In the first set of samples, NR and NR-Si solutions prepared using fresh dye were characterized. In the second, NR and NR-Si were extracted into chloroform solution from previously prepared 90% BTMOS films. The diffusion coefficients of these "liberated" dye molecules were then measured. Time transients (50-μs resolution, 3.3-s duration) for these samples were obtained by focusing into the bulk of each solution. The transients were autocorrelated as defined in eq 3 and fit to a modified form of eq 4,[23] assuming a focus depth of 2s. In all cases, the bulk autocorrelation decays could be fit well to a single-component diffusional decay (i.e., $A_2 = 0$ in eq 4).

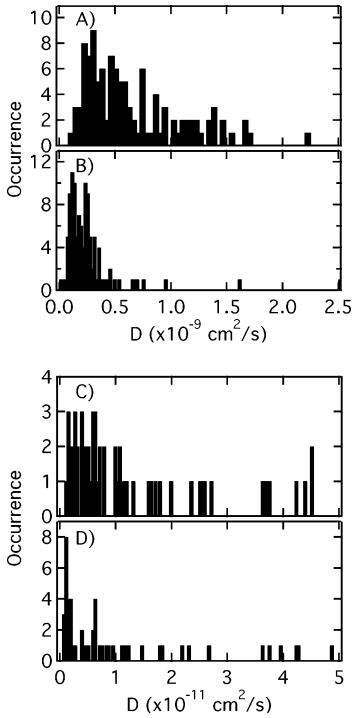

Figure 5. Histograms of the diffusion coefficients derived from fits of more than 100 autocorrelations for each 90% BTMOS sample. (A, B) Diffusion coefficient distributions for the fast components (D_1) of the autocorrelation decays for NR and NR-Si, respectively. (C, D) Diffusion coefficients derived from the slow-decay components (D_2) for NR and NR-Si, respectively.

Fresh NR in chloroform yielded $D = (1.9 \pm 0.3) \times 10^{-6}$ cm^2/s, while fresh NR-Si yielded $D = (1.8 \pm 0.3) \times 10^{-6}$ cm^2/s. The similarity in diffusion coefficients for fresh NR and NR-Si is expected since the addition of the alkyltriethoxysilane moiety to the NR structure does not significantly change the size of the molecule. In contrast, the diffusion coefficients for the NR and NR-Si species "liberated" from the silicate (90% BTMOS) films were significantly different, exactly as observed in the single-molecule/single-point measurements on the films. Specifically, the "liberated" NR and NR-Si yielded $D = (2.2 \pm 0.2) \times 10^{-6}$ cm^2/s and $D = (1.0 \pm 0.1) \times 10^{-6}$ cm^2/s, respectively. The absolute values of these diffusion coefficients may include some systematic error as the exact size of the detection area in these experiments is not known. However, the relative magnitudes of the diffusion coefficients is obtained accurately. As in the silicate film data presented above, the diffusion coefficients of the "liberated" NR and NR-Si species differ from each other by a factor of ~2.2, indicating that the "liberated" NR-Si species differs in size from NR. This size difference is attributed here to the binding of NR-Si to silicate oligomers.

(46) Schenter, G. K.; Lu, H. P.; Xie, X. S. *J. Phys. Chem. A* **1999**, *103*, 10477.

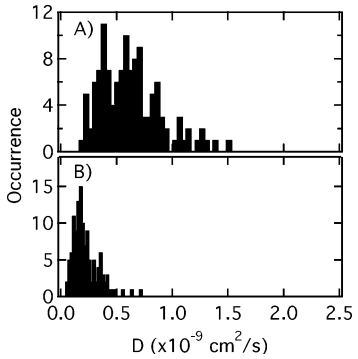

Figure 6. Histograms of diffusion coefficients (D_1) derived from simulated fluorescence time transients. Results are reported for simulations employing diffusion coefficients of (A) $D = 4.0 \times 10^{-10}$ cm^2/s and (B) $D = 1.5 \times 10^{-10}$ cm^2/s.

The ratios of the diffusion coefficients obtained from the NR and NR-Si-doped films (and from the bulk solutions) can be used to estimate the size and mass of the silicate oligomers to which the NR-Si molecules are bound. As a first approximation, this can be accomplished via the Stokes−Einstein relation, which states that the diffusion coefficient of a spherical object is inversely related to its radius. An approximately 3-fold reduction in D for the NR-Si molecules (relative to NR) indicates the silicate oligomers may be 3 times larger (in radius) than NR itself. The particle mass then scales as the cube of the radius, yielding an upper bound to the mass of 27 times that of NR, or 8600 g/mol. However, it is not likely the silicate oligomers are spherical in shape. While their exact shape is unknown, D is often taken to be inversely proportional to the square root of the mass in empirical relationships describing diffusion of organic polymers.[47] Hence, a lower bound for the mass may be estimated at 9 times that of NR or 2900 g/mol. This latter model assumes the oligomers take on a more extended-chain geometry.

Evaluation of Sample Heterogeneity. Single-molecule spectroscopy can also provide valuable information on the heterogeneity of the present samples. Evidence for the formation of inorganic- and organic-rich domains in silicate films derived from mixtures of TEOS and various organoalkoxysilanes has been reported previously.[31−36] As a result, heterogeneity in the rate of molecular diffusion[20] through the present films is expected. The broad distribution shown in Figure 5A for NR in the 90% BTMOS films might be reflective of such heterogeneity. This same distribution also exhibits a profound tail to higher diffusion coefficients. Interestingly, the NR-Si-doped samples (Figure 5B) yield a distribution that is much narrower.

Simulated time transients[26] were employed to help interpret the NR-Si and NR histograms in terms of sample heterogeneity. In these studies, time transients for perfectly homogeneous samples were numerically generated, autocorrelated and fit using eq 4 in a manner identical to the analysis of the experimental data. The results provide a view of the variations expected in the experimentally determined diffusion coefficients from uncertainties in the autocorrelations and their fits. Figure 6 depicts the distribution of D values (fast component) obtained.

For these simulations, 180 molecules were positioned randomly in a 30 × 30 μm region. The number of molecules present was kept constant by having molecules that diffuse out of one edge of the region "wrap around" to reenter on the opposite side. At each time slice, Δt, each molecule was displaced from its previous position by a step of random size. The step size probability distribution was a Gaussian with a mean-square width of $2D\Delta t$ in each direction (two dimensions). The excitation spot was positioned at the center of the 30 × 30 μm region and had a variance, s^2, of 4×10^{-10} cm^2. The maximum signal from each single molecule was set to 200 counts/10 ms. A background signal equivalent to 20% of the signal expected from a single molecule was added to each transient. Random variations were added to the signal and background counts to simulate the effects of shot noise. Two separate simulations were performed. In one, each molecule was assigned a diffusion coefficient of 4×10^{-10} cm^2/s (Figure 6A), similar to the measured D_1 for NR. In the other, the diffusion coefficients were all set to 1.5×10^{-10} cm^2/s (Figure 6B), similar to the measured D_1 for NR-Si. A total of 125 transients were simulated in each case. The simulated transients were exactly the same lengths as those acquired experimentally (i.e., 670 s for NR and 1340 s for NR-Si).

The similarities in the widths and shapes of the experimental and simulated histograms shown in Figure 5A,B and Figure 6, respectively, indicate that the widths of the fast diffusion coefficient distributions (D_1) depicted in Figure 5A,B are limited by uncertainties associated with the autocorrelation and fitting procedures. That is, the distribution widths do not reflect sample heterogeneity in this case.

Distinct differences between the experimental and simulated data do exist, however. Most notably, the majority of experimental autocorrelations required two diffusional decay components for proper fitting (see eq 4), while far fewer of the simulated time transients required such accommodations. Specifically, only 20% of the simulated data for $D = 4 \times 10^{-10}$ cm^2/s required inclusion of the slow diffusional component, compared to 67% of the experimental transients. Likewise, only 14% of the simulated data for $D = 1.5 \times 10^{-10}$ cm^2/s required this second, slow component, compared to 50% of the experimental transients.

The appearance of the two decay components in the experimental data is attributed here to sample heterogeneity on length scales similar to or smaller than the size of the excitation spot. Such heterogeneity is manifested as temporal variations in the diffusion coefficient within each transient but not necessarily as spatial variations between individual transients. The distributions shown in Figure 5C,D reflect an ~100-fold reduction in the rate of dye diffusion (i.e., $D_2 \approx D_1/100$). The two diffusional components likely result from the phase separation of organic- and inorganic-rich film regions.[31−36] The dye likely moves more slowly or may become briefly immobilized in the inorganic-rich regions.[23] Diffusion of the molecules through (or with) liquidlike silicate oligomers present in organic-rich film regions would yield relatively more rapid diffusion.

CONCLUSIONS

In summary, single-molecule spectroscopic methods have been used to study diffusion in thin ORMOSIL films prepared by the sol−gel process. Results for the diffusion of "free" and silicate-bound dye molecules were obtained. Surprisingly, both molecules showed relatively facile diffusion with the average diffusion

(47) Sun, S. F. *Physical Chemistry of Macromolecules. Basic Principles and Issues*; John Wiley & Sons: New York, 1994.

coefficient associated with fast diffusion of the silicate-bound molecules only ~3−4 times smaller than that of the "free" dye. These results were taken as clear evidence for the presence of silicate oligomers in the films. Bulk solution-phase FCS studies of dye molecules "liberated" from the silicate films provided important support for these conclusions. Heterogeneity in the films was manifested through the observation of two distinctly different time scales for single-molecule diffusion. The origin of the two components was attributed to the presence of inorganic- (slow diffusion) and organic-rich (fast diffusion) domains. Such results are important to those developing similar materials for use in catalysts and chemical sensors. The presence of liquidlike oligomers facilitates diffusion of reactants/analytes through these materials and may therefore enhance the activity/response of devices based upon ORMOSIL thin films.

ACKNOWLEDGMENT

The authors thank the National Science Foundation (CHE-0316466), the Army Research Office, and the State of Kansas for support of this work.

SUPPORTING INFORMATION AVAILABLE

Additional images and image autocorrelations to augment the discussion associated with Figure 3 and examples of the bulk solution-phase time transients and autocorrelations for the "liberated" dyes. This material is available free of charge via the Internet at http://pubs.acs.org.

Received for review June 9, 2004. Accepted October 20, 2004.

AC0491511